PHYSICAL MODELING OF VOLTAGE-DRIVEN RESISTIVE SWITCHING IN OXIDE RRAM

Daniele Ielmini*, Stefano Larentis and Simone Balatti

Dipartimento di Elettronica e Informazione
Politecnico di Milano and IU.NET, piazza L. da Vinci 32
Milano, Italy
*ielmini@elet.polimi.it

Abstract—**Resistive switching random access memory (RRAM) offers fast switching, high endurance and CMOS-compatible integration. Although functional devices below 10 nm have been already demonstrated, assessing the ultimate scaling of RRAM requires a detailed understanding and modeling of switching and reliability processes. This work discusses the modeling of bipolar switching in RRAM. An analytical model is first introduced to describe the temperature- and field-accelerated growth of the conductive filament (CF) induced by ion migration. The analytical model accounts for time-resolved data of the set transition, highlighting the central role of voltage as the driving parameter for set/reset transitions. The analytical model also accounts for the switching parameters as a function of the compliance current. A numerical model is then presented, allowing for a detailed description of the gradual increase during the reset transition. The numerical model highlights the different CF morphology in programmed states obtained by either set or reset. The improved insight into the switching process and the newly developed simulation tools enable device design, reliability prediction and materials engineering in RRAM.**

I. INTRODUCTION

Flash memory scaling has allowed improvement of bit density and decrease of the cost per bit in nonvolatile memories during the past decades. Since the conventional planar floating-gate cell is expected to face severe limitations for its scaling beyond the 10 nm node [1], new memory concepts based on materials storage are being investigated. Among these technologies, the resistive switching memory (RRAM) [2] has demonstrated a downscaling capability in the single-digit nanometer range [3]. Also, RRAM may find application opportunities in RAM and computation thanks to its sub-ns switching [4,5] and extensive cycling endurance [6,7]. However, the ultimate scaling limitations and the potential reliability issues of RRAM have not yet been investigated in detailed. To this aim, the physics of resistive switching must be thoroughly understood and modeled.

Physical models for RRAM switching have already been proposed for both unipolar [8-11] and bipolar switching [12-20]. Bipolar switching has been described by oxygen radial diffusion [15], oxygen vacancy generation/recombination [16], quantum point contact transport [17, 18] and ion migration induced by the local field and temperature at a localized filament [12-14, 19, 20]. While most of the models provide a satisfactory explanation of the fundamental switching characteristics, extensive model validation against a variety of experimental evidences has yet to be shown.
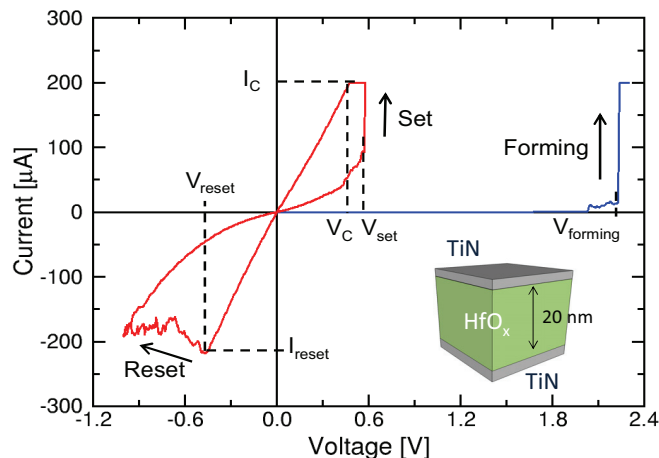

Fig. 1. Measured I-V curves for a HfO$_x$ RRAM during forming, set and reset transitions. The current during the forming and set operation at positive voltage was limited to a compliance level I$_C$ = 200 μA. Definition of the set voltage V$_{set}$, reset voltage V$_{reset}$, reset current I$_{reset}$ and corner voltage V$_C$ are also shown. The inset schematically shows the RRAM sample with a 20 nm-thick HfO$_x$ switching layer between TE and BE made of TiN.

This work discusses bipolar switching in the frame of ion migration, describing an analytical model [12, 13] and a numerical model [19, 20] for switching. The simulation results of the models are compared to switching characteristics for HfO$_x$-based RRAM devices [21-23]. The analytical model is used to account for voltage-driven switching characteristics during the set and reset transition. The limits of the analytical model in describing the details of the reset transitions are discussed, and a numerical model is introduced to overcome such limitations. The numerical model allows to account for the radically different morphology of set and reset states and for the switching kinetics during the reset transition. The numerical model thus provides a physically-accurate tool for device design and reliability prediction in RRAM.

II. VOLTAGE-DRIVEN BIPOLAR SWITCHING

Fig. 1 shows the measured I-V characteristics during forming, set and reset transitions in a RRAM devices with a HfO$_x$ switching layer. The RRAM device is schematically shown in the inset, and is characterized by a 20 nm-thick oxide layer and by TiN as top electrode (TE) and bottom electrode (BE) material [22-24]. Resistive switching is initialized by the forming operation at a voltage of more than 2 V. During the
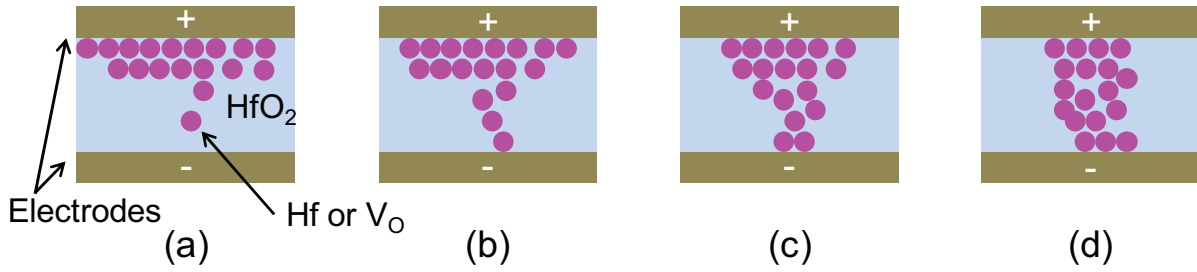
Fig. 2. Schematic illustration of the set transition in bipolar switching. In the initial reset state the CF is interrupted by the presence of a depleted gap (a). Application of a positive voltage to the TE induces migration of positively-ionized defects toward the gap, leading to the nucleation (b) and the subsequent growth of the CF (c, d) [12].

forming process, the current was limited to a compliance current I_C = 200 µA to avoid destructive breakdown. The forming operation introduces a conductive filament (CF) shunting the TE and the BE and inducing a low-resistance state (LRS) or set state of the RRAM. After forming, the CF can be deactivated by the reset operation under negative bias, where the resistance displays a gradual increase toward the high-resistance state (HRS) or reset state. Then, the application of a positive voltage sweep results in the set transition, appearing as an abrupt increase of the current to the set state. The voltage values for the onset of the set and reset transitions are called V_{set} and V_{reset}, respectively where $V_{reset} \approx -0.45$ V and $V_{set} \approx 0.6$ V in Fig. 1. Note that in the set transitions, the current is limited to I_C = 200 µA (same value as in the forming process) to allow a tight control of the resistance R in the set state and of the reset current I_{reset} [12, 13]. As a result of the constant current in the final stages of the set process, a voltage snap-back occurs. The corner voltage V_C = 0.4 V marks the boundary between the constant current regime at I_C and the decreasing voltage regime dictated by the applied sweep.

III. ANALYTICAL MODEL OF BIPOLAR RRAM

Fig. 2 schematically illustrates the physical mechanism for the set transition [12, 13]. In the initial reset state (a), the conductive defects (*e.g.* oxygen vacancies and/or excess metal atoms) responsible for the low resistance in the CF are separated by a gap as a result of the previous reset operation. Application of a positive voltage to the top electrode drives the positively-ionized defects toward the bottom electrode, thus resulting in the nucleation of the CF across the gap (b), followed by the growth of the CF diameter ϕ. The growth of the CF through ion migration can be described by the rate equation:

$$\frac{d\phi}{dt} = Ae^{-\frac{E_A}{kT}},\qquad(1)$$

where A is a pre-exponential factor, E_A is the activation energy for the growth process, k is the Boltzmann constant and T is the local temperature. The activation energy in Eq. (1) can be viewed as the energy barrier for ion hopping, which is the limiting process of the growth process. The energy barrier for ion hopping is in fact controlled by the voltage according to [12, 13]:

$$E_A = E_{A0} - \alpha qV,\qquad(2)$$

where α is a constant and V is the voltage across the device. On the other hand, the temperature is locally enhanced through the Joule heating induced by the current flowing through the CF [8, 9, 11-14]. The local temperature can be analytically estimated using the formula for the maximum temperature along a wire with uniform resistivity and assuming that the TE and BE behave as ideal heat sinks [12]. Based on this approximation, the local temperature reads:

$$T = T_0 + R_{th}V^2/R,\qquad(3)$$

where R_{th} is the effective thermal resistance of the CF [12]. Eqs. (1-3) allow to calculate the CF diameter and resistance for increasing time during the set transition. The reset transition can be similarly described by changing the sign of the right hand side in Eq. (1) from positive to negative, resulting in a decrease of ϕ due to ion migration back to the TE reservoir.

A. Time Dependence of CF Growth

To validate the analytical model in the set transition, we measured the resistance as a function of time during set in HfO$_x$-based RRAM. In the set operation, a voltage V_A was applied to the RRAM device initially in the reset state (R ≈ 5 kΩ) in series with a load resistance R_L. Fig. 3 shows the measured R as a function of time during set, for increasing R_L = 1 kΩ (a), 2.2 kΩ (b) and 5 kΩ (c) [13, 25]. The decrease of R can be understood by the increasing filament diameter as in Fig. 2. The CF growth is accelerated for increasing V_A, since a larger voltage induces a lower migration barrier and a higher local temperature, thus enhancing the ion-migration rate. As R_L is increased from Fig. 3a to c, the growth process saturates to a smaller diameter, hence larger R.

Fig. 3 also shows the calculation results according to the analytical model in Eqs. (1)-(3). Calculations were obtained for E_A = 1.2 eV, A = 1 ms^{-1} and α = 0.3. The model reproduces the correct dependences on time, V_A and R_L of the measured R. Most interestingly, Figs. 3e-g show the measured voltage across the device V as a function of time. It can be seen that V always readjusts to the same value for any given time, *e.g.* about 0.6 V after 10 µs, irrespective of V_A and R_L. This is the signature of a voltage-driven process, where the growth rate is a strong function of the voltage across the device, controlling the barrier lowering and the local temperature according to Eqs. (2) and (3), respectively. Note that voltage V at 1 s, namely the end of the set transition in Fig. 3, is approximately equal to 0.4
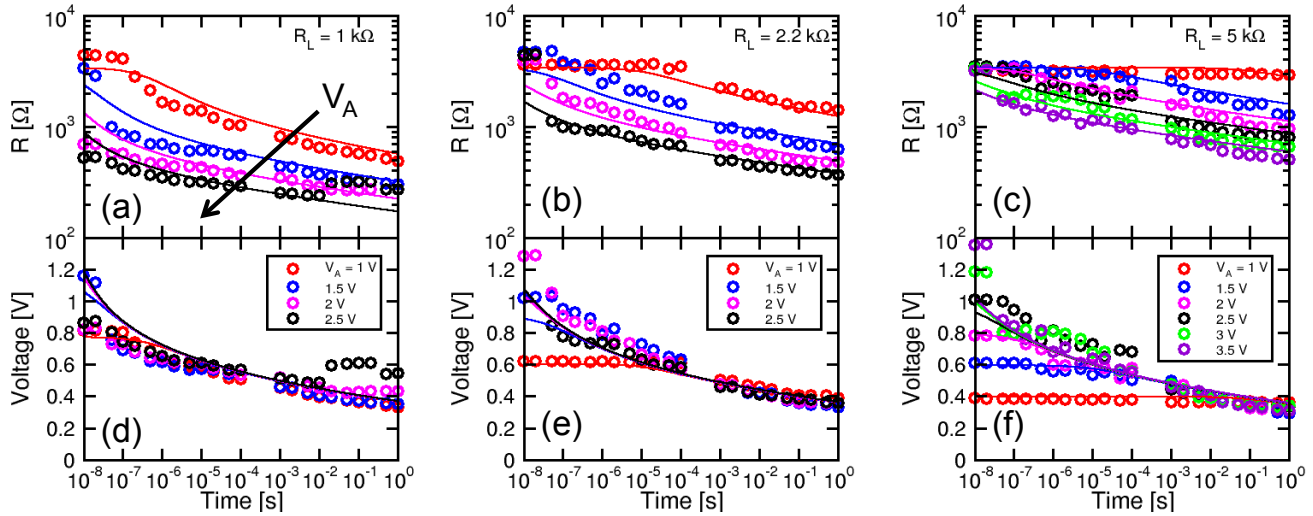
Fig. 3. Measured and calculated resistance during the set transition for variable load resistance R_L in series to the RRAM device, namely $R_L = 1$ kΩ (a), 2.2 kΩ (b) and 5 kΩ (c). The corresponding voltage across the device is shown in (d-f). The decreasing resistance reflects the growth of the CF. As V_A is increased, the set transition to low R shifts to shorter times, due to the voltage-activation of the set process. Note that the voltage in (d-f) follows a universal evolution with time irrespective of V_A and R_L, thus supporting a voltage-driven kinetic for CF growth during set transition [25].

V. This is consistent with the corner voltage V_C at the end of the set transition (typically around 1 s) at constant current I_C in Fig. 1. Therefore, the corner voltage V_C measured in DC-type I-V characteristics can be understood as the 'natural' voltage across the growing CF at about 1 s according to the universal voltage evolution with time in Fig. 3 [25].

B. I_C-dependence of set and reset characteristics

The analytical model can also account for the control of the set-state resistance R and of the reset current I_{reset} through adjustment of the current compliance I_C [12, 13]. Fig. 4 shows the measured R (a) and I_{reset} (b) as a function of I_C, for several metal oxides, including NiO [26, 27], HfO$_x$ [22, 28], HfO$_x$/ZrO$_x$ [29] and TiO$_x$ [30]. Note that most data in Fig. 4a follow the empirical law of constant $V_C = RI_C \approx 0.4$ V, while data in Fig. 4b obey the empirical law $I_{reset} \approx I_C$, irrespective of their unipolar [26, 27] or bipolar switching behavior [22, 28-30]. Calculations by the analytical model are also shown in the figure, for different $E_A = 0.9$, 1.2 and 1.5 eV. The constant V_C in Fig. 4a can be explained by the voltage-driven set transition, where the voltage across the device at a given time during the set transition do not depend on I_C [25]. It is useful to recall that all measurements in Fig. 4 were conducted in DC mode, with typical time scale in the one/few second range, thus $V_C = 0.4$ V is expected from the universal time evolution of V in Fig. 3. Data also display a negligible dependence of V_C on the active material, which can be understood by the small dependence on E_A in the calculations. The reset behavior with $I_{reset} = I_C$ can be explained by $V_{reset} = V_C$, namely the onset of ion migration under either polarity in the few-second range occurs at the same voltage. This clearly reveals that the set and reset transitions rely on the same microscopic process, namely ion migration induced by the local field and temperature.

Fig. 5 shows the measured and calculated I-V curve during reset transition for variable I_C. The comparison indicate that the analytical model can account for the resistance in the set state

R and for the onset of the reset transition (V_{reset} and I_{reset}) as a function of I_C. However, the model cannot account for the gradual reset transition in the measured I-V curve. The calculated abrupt transition to high resistance can be understood by the sudden decrease of ϕ as the critical temperature for ion migration is approached. Due to the difference between modeling and experimental results, we
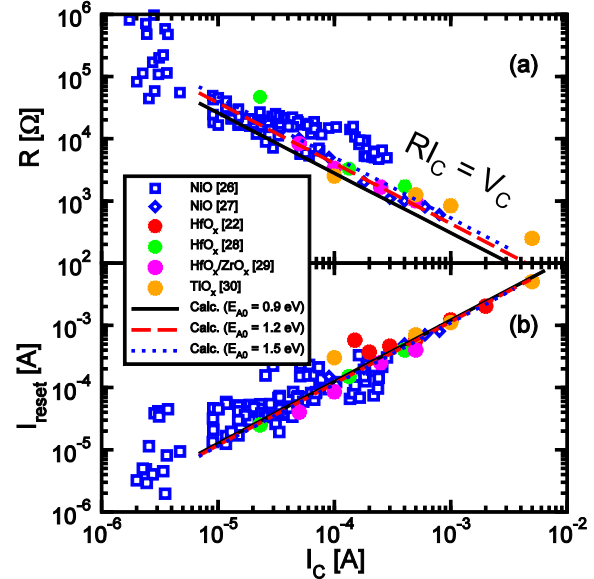

Fig. 4. Measured and calculated set-state resistance R (a) and I_{reset} (b) as a function of I_C. The constant product $RI_C = 0.4$ V in (a) originates from the constant voltage across the device $V_C = 0.4$ V at about 1 s in Fig. 3, which is due to the voltage-driven switching. The reset current equals the compliance current, due to the symmetry between switching voltages for set (V_C) and reset (V_{reset}) at equal time scale (about 1 s in the DC data in the figure). Data were obtained from different active oxides, including NiO [26, 27], HfO$_x$ [22, 28], HfO$_x$/ZrO$_x$ [29] and TiO$_x$ [30]. All data indicate similar V_C and obey $I_{reset} = I_C$, suggesting a universal set/reset behavior for all RRAM oxides [33].
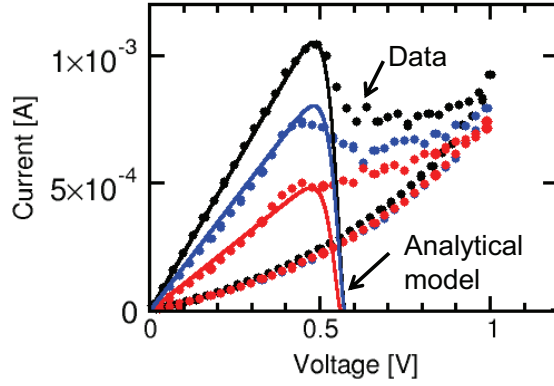
Fig. 5. Measured and calculated I-V curve during the reset transition under positive voltage. The previous set transition took place under negative voltage with variable I_C = 0.5, 0.75 and 1 mA. According to the analytical calculations, the resistance sharply increases in correspondence of the critical voltage V_{reset}, as a result of the exponential activation of CF dissolution in Eq. (1). On the other hand, data indicate a gradual increase of resistance.

conclude that the description based on a single parameter (ϕ) within the analytical model is too simplified to represent the CF evolution during the reset transition.

IV. NUMERICAL MODEL OF BIPOLAR RRAM SWITCHING

To identify the second geometrical parameter needed to represent the CF during the reset transition, we performed numerical simulations of ion migration [19]. In the numerical model, ion migration was described by the drift and diffusion phenomena of defects with concentration n_D. The numerical model solves the drift/diffusion equation:

$$\frac{\partial n_D}{\partial t} = \nabla \cdot (D\nabla n_D - \mu F n_D),\qquad (4)$$

where D is the ion diffusivity, μ is the ion mobility and F is the local field. Note that the diffusivity and the mobility control the diffusion and drift terms, respectively, namely the first and second terms in the right hand side of Eq. (4). Diffusivity and mobility were assumed to obey the Einstein relationship D = $\mu kT/q$, while both were dictated by the Arrhenius law:

$$D = D_0 e^{-\frac{E_A}{kT}},\qquad (5)$$

thus accounting for the strong temperature-acceleration of ion migration. An activation energy E_A = 1 eV, thus similar to the analytical model, was used in the numerical model. The drift-diffusion equation was solved consistently with the continuity equation for the electrical current and with the Fourier equation describing heat generation and heat transfer [19].

A. Reset Transition

Fig. 6 shows the measured and calculated I-V curves during the reset transition for two different initial set states at resistance R = 0.4 and 1 kΩ. in the figure, set transition was assumed to take place under negative voltage, thus the reset operation is shown for positive voltages applied to the TE. Calculations according to the numerical model now account well for the gradual increase of resistance above $V_{reset} \approx$ 0.4 V. To better understand the gradual reset transition within the numerical simulation, Fig. 7 shows the contour plot of the
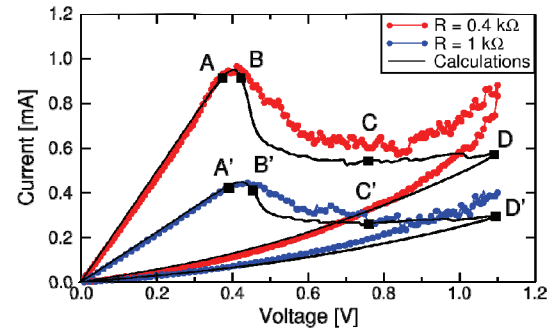

Fig. 6. Measured and calculated I-V curves for two different initial resistances R = 0.4 and 1 kΩ. The numerical model can account for the gradual reset transition, contrarily to the analytical model in Fig. 5.
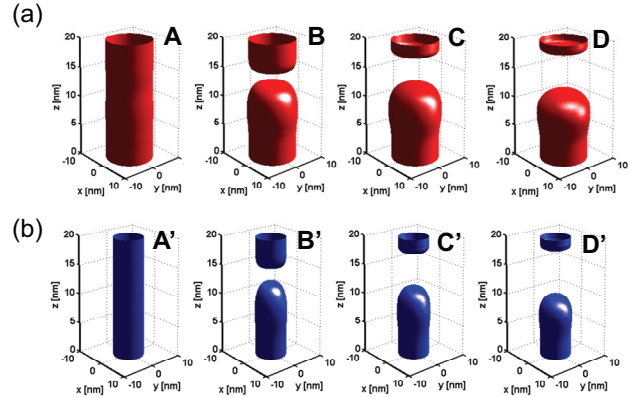

Fig. 7. Contour plot of the defect density corresponding to $n_D = 0.6 \times 10^{21}$ cm^{-3}, for the bias points A through D, for R = 0.4 kΩ, and A' through D', for R = 1 kΩ, along the reset transition in Fig. 6. The contour plot reveals the shape of the CF during reset, highlighting the gradual increase of the gap length for increasing voltage. The two different initial resistances in Fig. 6 were simulated by two different diameters of the CF.

defect concentration n_D obtained from the numerical simulations. The contour plots are shown at increasing voltage below/above V_{reset}, corresponding to the bias points A through D for the initial resistance R = 0.4 kΩ and A' through D' for the initial resistance R = 1 kΩ shown in Fig. 6. Contour plots were calculated from the concentration map of defects at a critical density of $n_D = 0.6 \times 10^{21}$ cm^{-3} and assuming an initial cylindrical shape of the CF [19]. Starting from a continuous CF morphology in A, a gap is gradually formed in the top region of the CF, as a result of the ion migration toward the BE in response to the application of a positive voltage to the TE. The depleted gap length increases for increasing voltage, thus resulting in the gradual increase of resistance in Fig. 6. The position of the gap is close to the middle of the CF, where the temperature peak is initially located. Note that a change in the CF shape (*e.g.* conical instead of cylindrical [31, 32]) would cause a shift of the hottest point, hence of the depleted gap, to one electrode or the other. Similar effects might be expected in case of substantial heating of the TE and/or the BE, due to non-ideal heat sinking. The latter might be expected in case of poor thermal conduction of the electrodes, or by the presence of a non-negligible thermal boundary resistance at the electrode/oxide interfaces. The gradual increase of the gap in
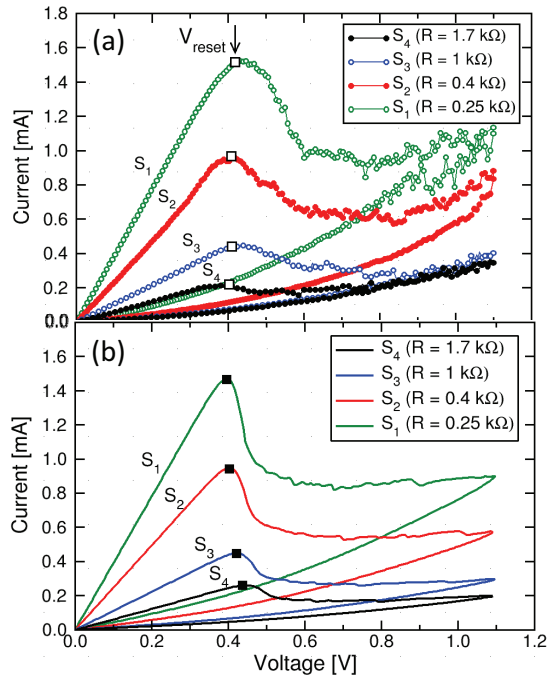
Fig. 8. Measured (a) and calculated (b) I-V curves showing the reset transition for set states with different initial resistance values, namely R = 0.25 kΩ (S$_1$), 0.4 kΩ (S$_2$), 1 kΩ (S$_3$) and 1.7 kΩ (S$_4$). Set states with different resistance were obtained by set operations at variable compliance current I$_C$. Both data and calculations indicate that the reset voltage V$_{reset}$ remains roughly constant at about 0.4 V, irrespective of the initial resistance.
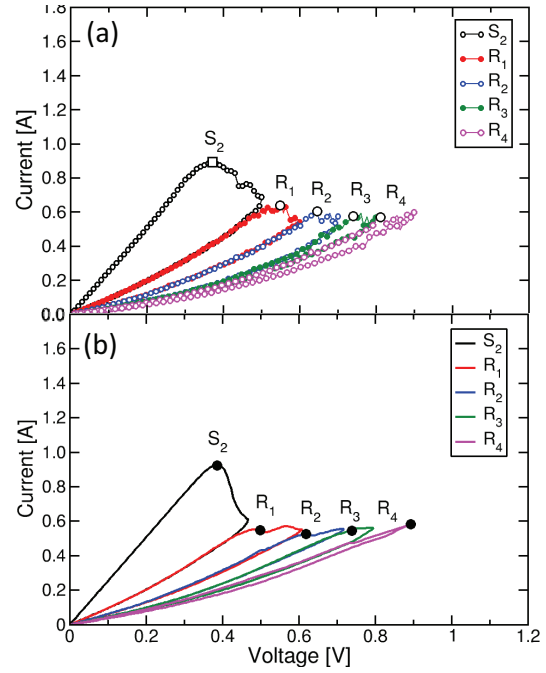

Fig. 9. Measured (a) and calculated (b) I-V curves showing the reset transition for reset states with different initial resistance values. Starting from the initial set state S$_2$ with a resistance R = 0.4 kΩ, incremental reset sweeps are applied, each sweep stopping at a larger voltage V$_{stop}$ from 0.5 V to 0.9 V, resulting in reset states R$_1$ through R$_4$. The reset voltage V$_{reset}$, defined as the onset of the reset transition for each state, increases with R, contrary to set states in Fig. 8.

Fig. 7 is due to a negative feedback loop, where an increasing gap results in a stronger localization of field and heating across the gap, thus resulting in smaller driving force for migration in the conductive regions of the CF [19]. This explains the strong differences between the abrupt set transition and the gradual reset transition, based on the positive and negative feedback effects, respectively. The fluctuations above V$_{reset}$ are due to the discrete mesh in the finite-element method (FEM) simulation: as soon as the temperature and field trigger ion migration at one mesh element in the top region of the filament, that element is suddenly depleted, thus resulting in a step change of resistance. Such 'migration burst' can account for the fluctuations which are generally observed in the measured I-V characteristics of RRAM above V$_{reset}$.

B. Set and Reset States

Based on the numerical simulations in Figs. 6 and 7, *reset states* achieved by a reset transition at a certain voltage are characterized by a voltage-dependent depleted gap as summarized in Fig. 7. On the other hand, the analytical model describing the filament diameter ϕ could properly account for *set states* obtained at variable time (Fig. 3) and at variable I$_C$ (Fig. 4). Set and reset states thus appear to have different morphologies, where set states correspond to a continuous CF with an effective diameter ϕ, while reset states are characterized by both a diameter and a depleted gap with length Δ. To experimentally validate this picture, Figs. 8 and 9 show the reset voltage V$_{reset}$ of set and reset states, respectively. Fig. 8a shows the measured I-V curves for the reset transition of set

states obtained by a DC set operation at increasing I$_C$. Four set states (S$_1$, S$_2$, S$_3$ and S$_4$) are shown in the resistance range between 0.25 kΩ and 1.7 kΩ. The states show decreasing R for increasing I$_C$, in agreement with data in Fig. 4a, and were simulated in Fig. 8b as continuous CFs with increasing diameter for increasing I$_C$. In both measurements and calculations, V$_{reset}$ remains constant and approximately equal to 0.4 V, irrespective of R. For comparison, reset states were studied in Fig. 9a according to the following procedure. First, a reset sweep between 0 V and V$_{stop}$ = 0.5 V > V$_{reset}$ was applied to the set state S$_2$ with R = 0.4 kΩ, thus resulting in the reset state R$_1$. A similar reset sweep with higher V$_{stop}$ = 0.6 V was then applied to R$_1$, allowing to obtain the reset state R$_2$ at higher resistance. The reset sweep applied to R$_1$ also allows for the measurement of V$_{reset}$ as the voltage for the onset of the reset transition toward higher resistance. Similar incremental reset sweeps were applied to generate states R$_3$ and R$_4$, and to measure the corresponding V$_{reset}$. Differently from set states, V$_{reset}$ increases for increasing R for reset states. Numerical simulations were conducted in Fig. 9b to replicate the experimental procedure of reset states formation starting from state S$_2$. The calculated V$_{reset}$ increases for increasing R of reset states, in agreement with experiments. Fig. 10 summarizes the measured and calculated V$_{reset}$ as a function of R for set and reset states. Reset states were obtained applying a reset sweep to either set state S$_2$ (R = 0.4 kΩ, same as Fig. 9) or state S$_3$ (R = 1 kΩ). Set states display a constant V$_{reset}$ = 0.4 V, with a small increase of V$_{reset}$ at decreasing R due to the additional voltage drop at a series resistance [33]. The constant V$_{reset}$ can
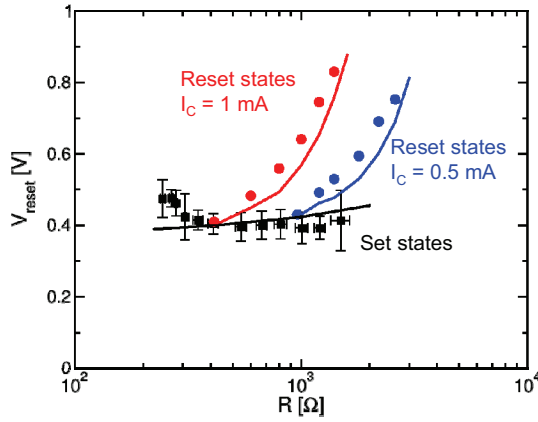
Fig. 10. Measured and calculated V_{reset} as a function of R for set and reset states. Data and calculations were obtained from Fig. 8 (set states) and Fig. 9 (reset states). Additional data for reset states obtained from a set state at R = 1 kΩ (I_C = 0.5 mA) are also shown. The reset voltage remains constant for set states, while V_{reset} increases at increasing R for reset states.
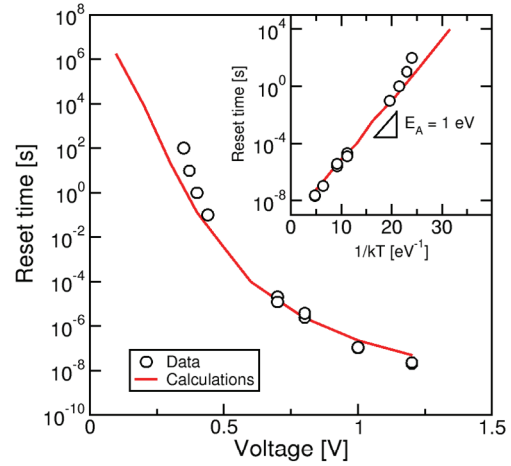

Fig. 11. Measured and calculated reset time as a function of the voltage across the RRAM device. The strongly non-linear voltage dependence allows fast switching and disturb immunity at the same time. The inset shows the same data/calculations as a function of 1/kT, where T was obtained as the maximum temperature along the CF in the calculations.

be explained by the continuous morphology of the CF, which results in an almost uniform field and a parabolic temperature profile along the CF. The temperature profile is independent of the CF diameter, thus the critical temperature for the onset of ion migration is the same irrespective of the CF diameter and R [34]. On the other hand, the field and heating is localized in the depleted gap for reset states, due to the larger resistivity and lower thermal conductivity at low defect density n_D [19, 20]. As a result, the field and temperature in the conductive regions of the CF decrease, thus reducing the driving force for ion migration. As a consequence, the reset voltage triggering ion migration increases for increasing gap length, or increasing R as shown in Fig. 10.

C. *Reset Kinetics*

The numerical model was validated against pulsed reset characteristics in Fig. 11. Here, the reset time is shown as a function of the voltage across the RRAM device. To evaluate the reset time, pulses with increasing duration were applied to a RRAM sample, initially programmed in the set state, leading to a resistance increase with time [19, 20]. The reset time was then defined in correspondence of a 60% increase of the resistance. The reset time in Fig. 11 strongly decreases for increasing voltage, supporting both low-voltage switching in the 10 ns time scale (voltage higher than 1.2 V) and a strong immunity to read disturb for voltages below 0.2 V. Simulation results account for the non-linear voltage dependence of reset time in the figure.

The large change of reset time in a relatively small voltage range is explained by the model in terms of Joule heating, as demonstrated by the Arrhenius plot in the inset of Fig. 11. Here, data and calculations plotted as a function of 1/kT, where T is the maximum temperature along the CF, appear as a straight line, thus suggesting that temperature serves as the main driving force for the reset process. The slope in the Arrhenius plot indicates an activation energy E_A = 1 eV, namely the value used in Eq. (5). Note that, if the field-induced barrier lowering was the main responsible for ion migration, one would expect an exponential relationship between reset

time and the applied voltage, according to Eq. (1). The non-exponential voltage dependence in the figure thus supports Joule heating as the critical driving force for RRAM switching [13, 14, 19, 20, 27].

V. CONCLUSION

Analytical and numerical models for oxide-based bipolar RRAM were presented and discussed. An analytical model is first developed, describing the growth of the CF diameter with time according to an Arrhenius law of the local temperature. The analytical model accounts for time-resolved set characteristics and for DC switching parameters as a function of the compliance current. The analytical model cannot capture the gradual increase of resistance along the reset transition, due to the simplified, one-parameter CF description. To overcome the limitations of the analytical model, a numerical model for the rigorous solution of the drift/diffusion equation for ion migration is introduced. The numerical model highlights the presence of a depleted gap in the CF after the reset operation, allowing for a comprehensive description of set and reset states. The numerical model accounts for set/reset characteristics for different set/reset states and under both DC and pulsed operation, thus providing a physically-accurate tool for design and simulation of bipolar RRAM devices.

REFERENCES

[1]   K. Prall, N. Ramaswamy, W. Kinney, K. Holtzclaw, X. Chen, J. Strand, R. Bez, "An Update on Emerging Memory: Progress to 2Xnm," IEEE International Memory Workshop (IMW), pp. 1-5, 2012.

[2]   H.-S. P. Wong, H.-Y. Lee, S. Yu, Y.-S. Chen, Y. Wu, P.-S. Chen, B. Lee, F. T. Chen, and M.-J. Tsai, "Metal-oxide RRAM," Proc. IEEE, vol. 100, pp. 1951-1970, 2012.

[3]   C.H. Ho, C.-L. Hsu, C.-C. Chen, J.-T. Liu, C.-S. Wu, C.-C. Huang, C. Hu, and F.-L. Yang, "9nm Half-Pitch Functional Resistive Memory Cell

with <1μA Programming Current Using Thermally Oxidized Sub-Stoichiometric WO$_x$ Film," IEDM Tech. Dig., pp. 436-439, 2010.

[4] H. Y. Lee, Y. S. Chen, P. S. Chen, P. Y. Gu, Y. Y. Hsu, S. M. Wang, W. H. Liu, C. H. Tsai, S. S. Sheu, P. C. Chiang, W. P. Lin, C. H. Lin, W. S. Chen, F. T. Chen, C. H. Lien, and M.-J. Tsai, "Evidence and solution of Over-RESET Problem for HfO$_x$ Based Resistive Memory with Sub-ns Switching Speed and High Endurance," IEDM Tech. Dig., pp. 460-463, 2010.

[5] A. C. Torrezan, J. P. Strachan, G. Medeiros-Ribeiro and R. S. Williams, "Sub-nanosecond switching of a tantalum oxide memristor," Nanotechnology, vol. 22, pp. 485203, 2011.

[6] M.-J. Lee, C. B. Lee, D. Lee, S. R. Lee, M. Chang, J. H. Hur, Y.-B. Kim, C.-J. Kim, D. H. Seo, S. Seo, U-I. Chung, I.-K. Yoo, and K. Kim, "A fast, high-endurance and scalable non-volatile memory device made from asymmetric Ta$_2$O$_{5-x}$/TaO$_{2-x}$ bilayer structures," Nature Materials, vol. 10, pp. 625-630, 2011.

[7] J J. Yang, M.-X. Zhang, J. P. Strachan, F. Miao, M. D. Pickett, R. D. Kelley, G. Medeiros-Ribeiro, and R. S. Williams, "High switching endurance in TaO$_x$ memristive devices," Appl. Phys. Lett., vol. 97, pp. 232102, 2010.

[8] U. Russo, D. Ielmini, C. Cagli and A. L. Lacaita, "Filament conduction and reset mechanism in NiO-based resistive-switching memory (RRAM) devices," IEEE Trans. Electron Devices, vol. 56, pp. 186-192, 2009.

[9] U. Russo, D. Ielmini, C. Cagli and A. L. Lacaita, "Self-accelerated thermal dissolution model for reset programming in NiO-based resistive switching memory (RRAM) devices," IEEE Trans. Electron Devices, vol. 56, pp. 193-200, 2009.

[10] C. Cagli, F. Nardi and D. Ielmini, "Modeling of set/reset operations in NiO-based resistive-switching memory (RRAM) devices," IEEE Trans. Electron Devices, vol. 56, pp. 1712-1720, 2009.

[11] S. Larentis, C. Cagli, F. Nardi and D. Ielmini, "Filament diffusion model for simulating reset and retention processes in RRAM," Microelectron. Eng., vol. 88, pp. 1119-1123, 2011.

[12] D. Ielmini, "Modeling the universal set/reset characteristics of bipolar RRAM by field- and temperature-driven filament growth," IEEE Trans. Electron Devices, vol. 58, pp. 4309-4317, 2011.

[13] D. Ielmini, "Filamentary switching model in RRAM for time, energy and scaling projections," IEDM Tech. Dig., pp. 409-412, 2011.

[14] S. Menzel, M. Waters, A. Marchewka, U. Böttger, R. Dittmann, and R. Waser, "Origin of the Ultra-nonlinear Switching Kinetics in Oxide-Based Resistive Switches," Adv. Funct. Mater., vol. 21, pp. 4487-4492, 2011.

[15] G. Bersuker, D. C. Gilmer, D. Veksler, P. Kirsch, L. Vandelli, A. Padovani, L. Larcher, K. McKenna, A. Shluger, V. Iglesias, M. Porti, and M. Nafría, "Metal oxide resistive memory switching mechanism based on conductive filament properties," J. Appl. Phys., vol. 110, pp. 124518, 2011.

[16] X. Guan, S. Yu, and H.-S. P. Wong, "On the Switching Parameter Variation of Metal-Oxide RRAM—Part I: Physical Modeling and Simulation Methodology," IEEE Trans. Electron Devices, vol. 59, pp. 1172-1182, 2012.

[17] R. Degraeve, A. Fantini, S. Clima, B. Govoreanu, L. Goux, Y.Y. Chen, D.J. Wouters, Ph. Roussel, G.S. Kar, G. Pourtois, S. Cosemans, J.A. Kittl, G. Groeseneken, M. Jurczak, L. Altimime, "Dynamic 'Hour Glass' Model for SET and RESET in HfO$_2$ RRAM," Symp. VLSI Tech. Dig., pp. 75-76, 2012.

[18] E. Miranda, D. Jiménez and J. Suñé, "The Quantum Point-Contact Memristor," IEEE Electron Device Lett., vol. 33, pp. 1474-1476, 2012.

[19] S. Larentis, F. Nardi, S. Balatti, D. C. Gilmer and D. Ielmini, "Resistive switching by voltage-driven ion migration in bipolar RRAM – Part II: Modeling," IEEE Trans. Electron Devices, vol. 59, pp. 2468-2475, 2012.

[20] S. Larentis, F. Nardi, S. Balatti, D. Gilmer and D. Ielmini, "Bipolar-switching model of RRAM by field- and temperature-activated ion migration," IEEE International Memory Workshop (IMW), pp. 53-56, 2012.

[21] D. C. Gilmer, G. Bersuker, H-Y. Park, C. Park, B. Butcher, W. Wang, P. D. Kirsch, and R. Jammy, "Effects of RRAM Stack Configuration on Forming Voltage and Current Overshoot," IEEE International Memory Workshop (IMW), pp. 123-126, 2011.

[22] F. Nardi, S. Larentis, S. Balatti, D. C. Gilmer and D. Ielmini, "Resistive switching by voltage-driven ion migration in bipolar RRAM – Part I: Experimental study," IEEE Trans. Electron Devices, vol. 59, pp. 2461-2467, 2012.

[23] F. Nardi, S. Balatti, S. Larentis and D. Ielmini, "Complementary switching in metal oxides: toward diode-less crossbar RRAMs," IEDM Tech. Dig., pp. 709-712, 2011.

[24] F. Nardi, S. Balatti, S. Larentis, D. C. Gilmer and D. Ielmini, "Complementary switching in oxide-based bipolar resistive switching memory (RRAM)," IEEE Trans. Electron Devices, vol. 60, 2013. In press.

[25] D. Ielmini, F. Nardi and S. Balatti, "Evidence for voltage driven set/reset processes in bipolar switching RRAM," IEEE Trans. Electron Devices, vol. 59, pp. 2049-2056, 2012.

[26] F. Nardi, D. Ielmini, C. Cagli, S. Spiga, M. Fanciulli, L. Goux, and D. J. Wouters, "Control of filament size and reduction of reset current below 10 μA in NiO resistance switching memories," Solid State Electron., vol. 58, pp. 42-47, 2011.

[27] K. Tsunoda, K. Kinoshita, H. Noshiro, Y. Yamazaki, T. Iizuka, Y. Ito, A. Takahashi, A. Okano, Y. Sato, T. Fukano, M. Aoki, and Y. Sugiyama, "Low power and high speed switching of Ti-doped NiO ReRAM under the unipolar voltage source of less than 3 V," IEDM Tech. Dig., pp. 767-770, 2007.

[28] H. Y. Lee, P. S. Chen, T. Y. Wu, Y. S. Chen, C. C. Wang, P. J. Tzeng, C. H. Lin, F. Chen, C. H. Lien, and M.-J. Tsai, "Low power and high speed bipolar switching with a thin reactive Ti buffer layer in robust HfO$_2$ based RRAM," in IEDM Tech. Dig., pp. 297-300, 2008.

[29] J. Lee, J. Shin, D. Lee, W. Lee, S. Jung, M. Jo, J. Park, K. P. Biju, S. Kim, S. Park, and H. Hwang, "Diode-less nano-scale ZrO$_x$/HfO$_x$ RRAM device with excellent switching uniformity and reliability for high-density cross-point memory applications," in IEDM Tech. Dig., pp. 452-455, 2010.

[30] J. Park, S. Jung, J. Lee, W. Lee, S. Kim, J. Shin, and H. Hwang, "Resistive switching characteristics of ultra-thin TiO$_x$," Microelectron. Eng., vol. 88, pp. 1136-1139, 2011.

[31] K. M. Kim and C. S. Hwang, "The conical shape filament growth model in unipolar resistance switching of TiO$_2$ thin film," Appl. Phys. Lett., vol. 94, pp. 122109, 2009.

[32] D.-H. Kwon, K. M. Kim, J. H. Jang, J. M. Jeon, M. H. Lee, G. H. Kim, X.-S. Li, G.-S. Park, B. Lee, S. Han, M. Kim, and C. S. Hwang, "Atomic structure of conducting nanofilaments in TiO$_2$ resistive switching memory," Nature Nanotechnol., vol. 5, pp. 148-153, 2010.

[33] D. Ielmini, F. Nardi and C. Cagli, "Universal reset characteristics of unipolar and bipolar metal-oxide RRAM," IEEE Trans. Electron Devices, vol. 58, pp. 3246-3253, 2011.

[34] D. Ielmini, C. Cagli and F. Nardi, "Physical models of size-dependent nanofilament formation and rupture in NiO resistive switching memories," Nanotechnology, vol. 22, pp. 254022, 2011.